Eur. Phys. J. D **42**, 441–454 (2007)
DOI: 10.1140/epjd/e2007-00132-7

THE EUROPEAN PHYSICAL JOURNAL D

A fluid model of the current-voltage characteristics of an electron emitting electrode immersed in a two electron temperature plasma

T. Gyergyek[1,2,a] and M. Čerček[2,3]

[1] University of Ljubljana, Faculty of Electrical Engineering, Tržaška 25, 1000 Ljubljana, Slovenia
[2] Jožef Stefan Institute, Jamova 39, POB 100, 1000 Ljubljana, Slovenia
[3] University of Maribor, Faculty of Civil Engineering, Smetanova 17, 2000 Maribor, Slovenia

Received 24 May 2006 / Received in final form 29 September 2006
Published online 23 March 2007 –

Abstract. The current voltage characteristics of a negatively biased electron emitting electrode immersed in a two-electron temperature plasma are analyzed by a simple one dimensional fluid model. Based on the assumption that the electron density in the pre-sheath region obeys the Boltzmann law the Bohm criterion is derived in the form of a transcendental equation for the Mach number, which can have up to 3 solutions. According to these solutions the ion velocity at the sheath edge can be determined either by the hot or by the cool electron temperature. When it is determined by the cool electron temperature and the hot electron temperature is high enough the critical electron emission current from the collector can have a very pronounced local maximum and a minimum when regarded as a function of the electrode potential. Because of that the current voltage characteristics of the electrode may exhibit up to 3 different floating potentials. This result is in good agreement with the experimental observations reported in [J. Appl. Phys. **63**, 5674 (1988)].

PACS. 52.27.Cm Multicomponent and negative-ion plasmas – 52.40.Kh Plasma sheaths

1 Introduction

Emissive probes are a widely used plasma diagnostic tool [1] for the determination of the plasma potential in various plasma devices. An emissive probe is heated to a thermoelectron emitting temperature. When the probe bias is negative with respect to the plasma potential, the electron emission current flows from the probe to the plasma. This current can be decreased by space charge of negative electrons that can accumulate at the probe surface, if electron emission from the probe is too high. For a small electron emission and/or a strongly negative bias of the probe the potential distribution in the sheath remains monotonic, so that all emitted electrons are accelerated into the plasma. Such electron emission is called temperature limited emission, because the electron current from the probe into the plasma is limited by thermal emission of electrons from the probe surface. As the electron emission increases (when the temperature of the probe is increased), the electron accelerating electric field decreases and, eventually, the critical electron emission is reached when the electric field at the probe surface becomes zero and the condition for the so-called space charge limited emission is reached (Fig. 1). If the electron emission is further increased, a potential dip, a so-called virtual cathode, is created, which drives the emitted electrons back to the probe. Such emission is called supercritical. The problem of sheath formation in front of a negative electrode that emits electrons has been studied by several authors [2–7].

On the other hand the potential formation in plasmas containing energetic electrons has also been studied extensively [8–15], because plasmas with electron velocity distributions containing energetic tails are readily produced in many plasma machines for material processing as well as in laboratory and fusion devices. In these models energetic electrons are treated either as monoenergetic or thermal beams or as Maxwellian distributed electrons with higher temperature and lower density than the basic electron population. Attempts to treat simultaneously the effect of emitted and energetic electrons are more rare [7,15].

Recently the problem of the space charge limited emission current from a negative electrode has again been addressed by Takamura and coworkers [16–19]. They developed a one-dimensional fluid model, where they treated an infinitely large, planar, negative electrode (collector) that is immersed in plasma which contains a group of Maxwellian electrons and a group of cold singly charged positive ions. They assumed that the electrode emits monoenergetic electrons with zero initial velocity and that the flux of emitted electrons is proportional to the flux of

[a] e-mail: tomaz.gyergyek@fe.uni-lj.si

incoming electrons. The proportionality factor is assumed to be the constant emission coefficient.

In a recent paper [20] we have extended their model by the assumption that the hot electron population is present in the plasma, but the repulsion of the electrons in the pre-sheath potential drop was not taken into account. We have also allowed a non-zero initial velocity of the emitted electrons. The floating and the current collecting electrode were analyzed. In the next paper [21] the repulsion of the electrons in the pre-sheath potential drop was taken into account and the modification of the Bohm criterion in the form of a transcendental equation for the Mach number was derived. Only the floating electrode was analyzed. In this paper the study is somehow completed by the analysis of the current collecting electrode and in the same time taking into account the repulsion of electrons in the pre-sheath potential drop for the space charge limited and the temperature limited electron emission.

Because the model has previously been presented in 2 parts [20,21] the complete presentation of the model is given in a more concise form in the next section. In Section 3 some results of the model are shown. In Section 4 some conclusions are given.

2 Model

2.1 Basic assumptions and the Poisson equation

We consider an infinite plane material surface (collector), located at $x = 0$ in contact with a plasma filling the half-space $x > 0$ (Fig. 1). Far from the collector the plasma is quasi-neutral and the potential there is taken as a reference potential, which is set to zero, $\Phi = 0$. Also the electric field there is zero. The collector is biased to a certain potential Φ_C, which is negative and smaller (more negative) than $\Phi(x)$ for any $x > 0$. As one approaches the collector, the potential slowly decreases. This region of the slow potential drop is called the pre-sheath. There the plasma is assumed to be still quasi-neutral, although a small electric field exists in this region. This electric field accelerates the singly charged positive ions towards the collector and negative electrons in the opposite direction. The positive ions are assumed to be cold and at rest at a very large distance from the collector. In our model the very large distance from the collector means the region beyond the pre-sheath. At a certain distance $x = d$ from the collector, the plasma potential has a value Φ_S and there the ions reach the velocity v_0 in the direction towards the collector. The plane at $x = d$ is called the sheath edge. In our model the sheath thickness is much larger than the Debye length, i.e. $d \gg \lambda_D$, where λ_D is defined in (19), but in the same time d is much smaller than the characteristic length L of the pre-sheath, so we have $\lambda_D \ll d \ll L$. In the sheath the potential drops from the value Φ_S at the sheath edge to the value of the collector potential Φ_C.

We assume that there are two electron populations in the plasma. Both electron groups have Maxwellian velocity distribution with two different temperatures and zero

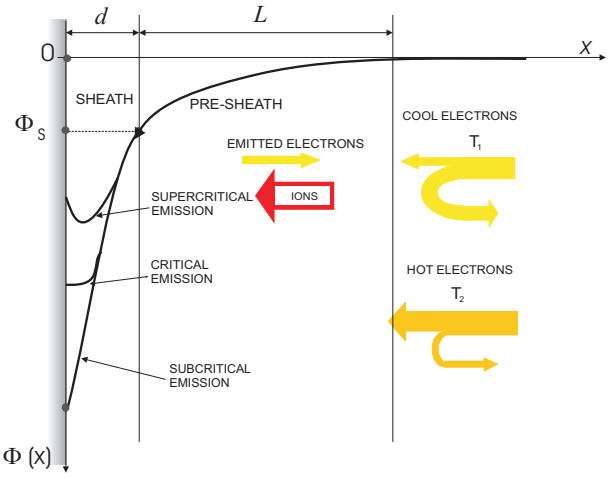

Fig. 1. Schematic of the model. The potential $\Phi(x)$ very far away from the collector is zero and at the sheath edge (at $x = d$) it is Φ_S. The pre-sheath length scale L is much larger than the sheath thickness d. When the emission is critical the electric field at the collector surface is zero.

average velocities. We call them the cool and the hot electrons. We also assume that the collector emits electrons. The emitted electrons are assumed to leave the collector all with the same initial velocity v_C, which in our model is allowed to be different from zero, and then they are accelerated by the potential in the sheath away from the collector.

The potential in the sheath $\Phi(x)$ is determined by the Poisson equation:

$$\frac{d^2\Phi}{dx^2} = -\frac{e_0}{\varepsilon_0}\left(n_i(x) - n_1(x) - n_2(x) - n_3(x)\right). \quad (1)$$

Here $n_i(x)$ is the ion density, $n_1(x)$ is the cool electron density, $n_2(x)$ is the hot electron density and $n_3(x)$ is the density of the emitted electrons in the sheath. The boundary conditions at the sheath edge are:

$$\Phi(x = d) = \Phi_S, \quad \frac{d\Phi}{dx}(x = d) \to 0. \quad (2)$$

The assumption that the electric field at the sheath edge is negligibly small is justified because of our approximation that $\lambda_D \ll d$.

The densities of the cool and of the hot electrons in the sheath are assumed to obey the Boltzmann relation:

$$n_1(x) = n_{1S} \exp\left(\frac{e_0(\Phi(x) - \Phi_S)}{kT_1}\right),$$
$$n_2(x) = n_{2S} \exp\left(\frac{e_0(\Phi(x) - \Phi_S)}{kT_2}\right). \quad (3)$$

Here n_{1S} and n_{2S} are the cool and the hot electron densities at the sheath edge, T_1 and T_2 are the cool and the hot electron temperatures, k is the Boltzmann constant and e_0 is the elementary charge. Note that in the sheath the electron velocity distribution function is actually a cutoff Maxwellian. At the distance x from the

collector ($x < d$) an electron that has almost reached the collector, but has then been repelled will have the velocity $\sqrt{2e_0\left(\Phi(x)-\Phi_C\right)/m_e}$ in the direction away from the collector. The electron density as a function of the potential is then obtained by the integration of such a velocity distribution function over the velocity. This gives the electron density in terms of the error function of the potential. Further analysis of the Poisson equation then requires the integration of error functions over the potential and this makes the model much more complicated. So we assume the Boltzmann distribution of the electrons in the sheath in order to keep the model as simple as possible.

At the sheath edge, the ion density is n_S and the velocity of the ions towards the collector is v_0. From the assumption of the ion flux and energy conservation the ion density in the sheath can be obtained:

$$n_i(x) = \frac{n_S}{\sqrt{1-\frac{2e_0(\Phi(x)-\Phi_S)}{m_i v_0^2}}}. \tag{4}$$

The emitted electrons are assumed to leave the collector all with the same initial velocity v_C. From the assumption of energy and flux conservation of the emitted electrons their density in the sheath $n_3(x)$ can be related to their density at the sheath edge n_{3S}:

$$n_3(x) = \frac{n_{3S}}{\sqrt{1-\frac{2e_0(\Phi(x)-\Phi_S)}{2e_0(\Phi_C-\Phi_S)-m_e v_C^2}}}. \tag{5}$$

The assumption that the sheath is collisionless is fully justified in our approximation where $d \ll L$.

We now introduce the following variables. The ion velocity at the sheath edge v_0 is written in the following form:

$$v_0 = M\sqrt{\frac{kT_1}{m_i}}. \tag{6}$$

The dimensionless parameter M is called the Mach number. The explanation for this will be given a little later in Section 2.2. In similar way we write down the velocity of the emitted electrons at the collector v_C:

$$v_C = N\sqrt{\frac{kT_1}{m_i}}. \tag{7}$$

The potentials at the sheath edge, in the sheath and at the collector are normalized to the cool electron temperature:

$$\Psi_S = \frac{e_0\Phi_S}{kT_1}, \quad \Psi = \frac{e_0(\Phi(x)-\Phi_S)}{kT_1},$$
$$\Psi_C = \frac{e_0(\Phi_C-\Phi_S)}{kT_1}. \tag{8}$$

At the sheath edge the plasma is quasi-neutral:

$$n_S = n_{1S} + n_{2S} + n_{3S}. \tag{9}$$

It is assumed that the ratio between the hot and the cool electron density at the sheath edge β_S is a given parameter:

$$\beta_S = \frac{n_{2S}}{n_{1S}}. \tag{10}$$

The electron emission from the collector may be either secondary or thermal. Secondary electron emission may be triggered by various kinds of impacting particles like electrons, ions and photons. The corresponding emission coefficients, which give the number of the emitted electrons per incident particle, depend on the energy and on the species of the impacting particle and on the material of the collector. Some related data can be found in e.g. [22] — chapter 4. If for example the collector is made of tungsten the emission coefficient is equal to 0.21 if the impacting ions are He^+, 0.30 for Ne^+, 0.09 for Ar^+ and 0.02 for Xe^+. For platinum and the ions H^+ and H_2^+ it is 3×10^{-3} for N^+ and N_2^+ it is 5×10^{-3} and for O^+ and O_2^+ it is 5×10^{-4}. These emission coefficients are almost independent of the energy of the impacting ions for energies up to 1 keV. Typical values for the electron emission coefficient introduced in equation (12) are between 0.4 and 1.6 for many metals and for the energies of the impacting electrons up to several keV. Because the electron emission coefficient is usually much larger than the emission coefficients for various ions, the ion contribution to the secondary emission is often neglected.

On the other hand the current density of the thermally emitted electrons is given by the Richardson formula:

$$j_R = A_R T_C^2 \exp\left(\frac{-e_0\Phi_w}{kT_C}\right), \tag{11}$$

where A_R is the Richardson constant, T_C is the absolute temperature of the collector, Φ_w is the work function of the collector and e_0 is the elementary charge. The theoretical value of the Richardson constant is $A_R = 4\pi m_e e_0 k^2/h^3 = 120\ \mathrm{A/(cm^2\,K^2)}$. Actual values for various metals are different. For example for tungsten the value is approximately 60 $\mathrm{A/(cm^2\,K^2)}$. The value of the work function for tungsten is approximately $e_0\Phi_w \approx 4.5$ eV.

In our model we include the secondary emission of electrons caused by the impacting ions, the secondary emission of electrons caused by the impacting electrons and the Richardson emission. The current density of the emitted electrons is therefore written as the sum of 3 contributions:

$$j_3 = \gamma_i j_i + \gamma\left(j_1 + j_2\right) + j_R. \tag{12}$$

Here γ_i is the secondary emission coefficient for the ions and γ is the secondary emission coefficient for the electrons.

Because all the fluxes are conserved in the sheath, we write down their values at the sheath edge:

$$j_1 = e_0 n_{1S}\exp\left(\frac{e_0(\Phi_C-\Phi_S)}{kT_1}\right)\sqrt{\frac{kT_1}{2\pi m_e}}, \tag{13}$$

$$j_2 = e_0 n_{2S}\exp\left(\frac{e_0(\Phi_C-\Phi_S)}{kT_2}\right)\sqrt{\frac{kT_{e2}}{2\pi m_e}}, \tag{14}$$

$$j_3 = e_0 n_{3S} v_{3S} = e_0 n_{3S} N\sqrt{\frac{kT_1}{m_i}}\sqrt{1-\frac{2e_0(\Phi_C-\Phi_S)m_i}{N^2 kT_1 m_e}},$$

$$j_i = e_0 n_S M\sqrt{\frac{kT_1}{m_i}}. \tag{15}$$

From equations (9)–(15) we get:

$$n_{1S} = n_S \frac{1 - \frac{J_R + M\gamma_i}{\sqrt{N^2 - \frac{2\Psi_C}{\mu}}}}{1 + \beta_S + G}, \quad n_{2S} = n_S \frac{\beta_S \left(1 - \frac{J_R + M\gamma_i}{\sqrt{N^2 - \frac{2\Psi_C}{\mu}}}\right)}{1 + \beta_S + G},$$
$$n_{3S} = n_S \frac{G + \frac{(1+\beta_S)(J_R + M\gamma_i)}{\sqrt{N^2 - \frac{2\Psi_C}{\mu}}}}{1 + \beta_S + G}. \tag{16}$$

The following variables have been introduced:

$$\mu = \frac{m_e}{m_i}, \quad \Theta = \frac{T_2}{T_1},$$
$$G = \frac{\gamma \left(\exp(\Psi_C) + \beta_S \sqrt{\Theta} \exp\left(\frac{\Psi_C}{\Theta}\right)\right)}{\sqrt{2\pi(N^2\mu - 2\Psi_C)}},$$
$$J_R = \frac{j_R}{e_0 n_S \sqrt{\frac{kT_1}{m_i}}}. \tag{17}$$

With the label G we follow the notation of Ye et al. [16,17]. If we put $\beta_S = N = 0$, (no hot electrons in the plasma and zero initial velocity of the emitted electrons) G defined in (17) becomes G defined by Ye et al. in [16].

Equations (3), (4), (5) and (16) are combined and inserted into the Poisson equation (1):

$$\frac{d^2\Psi}{dz^2} = \frac{1}{1 + \beta_S + G} \times \left(\begin{array}{l} \left(1 - \frac{J_R + M\gamma_i}{\sqrt{N^2 - \frac{2\Psi_C}{\mu}}}\right) \left(\exp(\Psi) + \beta_S \exp\left(\frac{\Psi}{\Theta}\right)\right) \\ \\ + \left(G + \frac{(1+\beta_S)(J_R + M\gamma_i)}{\sqrt{N^2 - \frac{2\Psi_C}{\mu}}}\right) \frac{1}{\sqrt{1 - \frac{\Psi}{\Psi_C - \frac{N^2\mu}{2}}}} \end{array} \right) - \frac{1}{\sqrt{1 - \frac{2\Psi}{M^2}}}, \tag{18}$$

where the normalized coordinate z has been introduced in the following way:

$$z = \frac{x}{\lambda_D}, \quad \lambda_D = \sqrt{\frac{\varepsilon_0 k T_1}{n_S e_0^2}}, \tag{19}$$

the normalized potential is defined in (8) and the normalized Richardson current density J_R is defined by (17).

2.2 The Bohm criterion

In this subsection we briefly discuss the general Bohm criterion, which represents a necessary condition for the existence of a sheath in the asymptotic limit considered here ($\lambda_D \ll d \ll L$), and use it to estimate the ion velocity at the sheath edge. The potential profile in the sheath is determined by the Poisson equation (1):

$$-\varepsilon_0 \frac{d^2\Phi}{dx^2} = \varrho(x) = e_0 \left(n_i(x) - n_1(x) - n_2(x) - n_3(x)\right), \tag{20}$$

where $\varrho(x)$ is the electric charge density in the sheath. At the sheath edge the boundary conditions (2) are imposed and also at the sheath edge the plasma is quasi-neutral: $\varrho(x = d) = 0$. So near the sheath edge the charge density can be Taylor expanded to the first order term:

$$\varrho(\Phi) = \varrho(x = d) + \Phi \left.\frac{d\varrho}{d\Phi}\right|_{\Phi = \Phi_S}. \tag{21}$$

When we insert (21) into (20), we obtain:

$$-\varepsilon_0 \frac{d^2\Phi}{dx^2} = \Phi \left.\frac{d\varrho}{d\Phi}\right|_{\Phi = \Phi_S}, \tag{22}$$

from which the condition for a non-oscillatory solution of equation (22) is found to be:

$$\left[\frac{d\varrho}{d\Phi}\right]_{\Phi \to \Phi_S} \leq 0.$$

This expression is usually referred to as the general Bohm criterion [24]. For non-divergent geometries, like in our case, the Bohm criterion is always satisfied in its marginal form, this means with the equality sign:

$$\left[\frac{d\varrho}{d\Phi}\right]_{\Phi \to \Phi_S} = 0,$$

or equivalently,

$$\left.\frac{dn_i}{d\Phi}\right|_{\Phi \to \Phi_S} = \left.\frac{dn_e}{d\Phi}\right|_{\Phi \to \Phi_S},$$

where

$$n_e = n_1 + n_2 + n_3 \tag{23}$$

is the electron density. Depending on how the ions and the electrons are treated (e.g. by fluid or kinetic models), the Bohm criterion assumes different special forms. For thermal ions and arbitrary electron density profiles $n_e(\Phi)$ the ion velocity at the sheath edge is given by [24]:

$$v_0 = \sqrt{\left.\frac{k(T_e^* + \kappa T_i)}{m_i}\right|_{x=d}}, \tag{24}$$

where κ is the polytropic coefficient and T_e^* is the electron screening temperature defined as [24,25]:

$$T_e^* = \frac{e_0 n_e}{k \frac{dn_e}{d\Phi}}. \tag{25}$$

We now insert (3) and (5) together with (16) into (23). The obtained electron density $n_e(\Phi)$ is then differentiated with respect to Φ. Both $n_e(\Phi)$ and $dn_e/d\Phi$ are the inserted into (25) and the screening temperature T_e^* is calculated. Then T_e^* and $T_i = 0$ are inserted into (24) and calculated

at the sheath edge $x = d$. Using the variables defined in (6), (8), (10) and (17) equation (24) becomes:

$$M = \sqrt{\frac{1+\beta_S+G}{\left(1-\frac{J_R+M\gamma_i}{\sqrt{N^2-\frac{2\Psi_C}{\mu}}}\right)\left(1+\frac{\beta_S}{\Theta}\right)+\frac{G+\frac{(1+\beta_S)(J_R+M\gamma_i)}{\sqrt{N^2-\frac{2\Psi_C}{\mu}}}}{2\left(\Psi_C-\frac{N^2\mu}{2}\right)}}}. \quad (26)$$

Note that if there are no hot electrons ($\beta_S = 0$) and no emitted electrons ($\gamma_i = G = J_R = 0$), then equation (26) gives $M = 1$, which is the "usual" Bohm criterion. If only the hot electrons are present ($\beta_S > 0$), but there is no electron emission from the collector $\gamma_i = G = J_R = 0$, the equation (26) is identical to the modified Bohm criterion derived by Takamura [9]. When γ_i is not zero, equation (26) is a third order equation for M.

2.3 Potential drop in the pre-sheath

Note that β_S is the hot to cool electron density ratio at the sheath edge. One may expect that this ratio is not the same at the sheath edge and in the unperturbed plasma beyond the pre-sheath region. By the assumption of our model the potential in the pre-sheath decreases monotonically from $\Phi(x) = 0$ at $x \geq L$ to $\Phi(x) = \Phi_S$ at $x = d$. Therefore part of the cool and of the hot electrons that move towards the collector are repelled from it back into the plasma by this potential drop. It is to be expected that a larger fraction of the cool electrons than of the hot electrons will be repelled by the potential drop in the pre-sheath. In order to calculate the density decrease of both electron populations from the unperturbed plasma to the sheath edge, we would have to solve the full scale plasma-sheath matching problem [23] for a plasma with 3 electron populations. This is far beyond the scope of this paper. But because we need a relation between the ion sound velocity v_0 at the sheath edge and the pre-sheath potential drop Φ_S we need to briefly sketch the lines along which such a problem could be treated.

The analysis we have presented so far has been done on the so-called sheath scale, where the possible collisions, ionizations and effects of non-planar geometry inside the sheath can be neglected, because the sheath is much thinner than the characteristic length scale of the pre-sheath, $d \ll L$. On the other hand treatment of the pre-sheath region is rather complicated because it involves the full difficulty of an inhomogeneous plasma in a self-consistent field. For a more detailed discussion of this problem the reader is referred to Section 5 of the review paper of Riemann [24]. The pre-sheath region may in some cases include the entire plasma body — e.g. in the collisionless plasma column. In other cases the pre-sheath region may be small compared to the entire plasma, like e.g. the Knudsen layer of a collision dominated plasma. In any case the dimension of the pre-sheath is always such that it must be quasi-neutral and the problem must be treated on the so called plasma scale, where the possible collisions, ionizations and effects of non-planar geometry must not be a-priori neglected. In the quasi-neutral pre-sheath the neutrality condition must be fulfilled:

$$n_i(x) - n_{10}\exp\left(\frac{e_0\Phi(x)}{kT_1}\right) - n_{20}\exp\left(\frac{e_0\Phi(x)}{kT_2}\right) - n_3(\Phi(x)) = 0. \quad (27)$$

In the plasma-sheath analysis the electron density is usually assumed to be a known function of the potential. For the hot and the cool electrons we have assumed that they both obey the Boltzmann relation also in the pre-sheath, not only in the sheath. Dependence of the density of the emitted electrons on the potential $n_3(\Phi(x))$ is also assumed to be a known function, but it does not have to be specified because it is not essential for our present analysis. So the cool and the hot electron densities n_{1S} and n_{2S} at the sheath edge and the respective electron densities n_{10} and n_{20} at $x \geq L$ are related by:

$$n_{1S} = n_{10}\exp(\Psi_S), \quad n_{2S} = n_{20}\exp\left(\frac{\Psi_S}{\Theta}\right). \quad (28)$$

We define the hot to cool electron density ratio β_0 at $x \geq L$ by:

$$\beta_0 = \frac{n_{20}}{n_{10}}. \quad (29)$$

From (29), (28) and (10) one obtains:

$$\beta_S = \beta_0\exp\left(\frac{\Psi_S(1-\Theta)}{\Theta}\right). \quad (30)$$

Note that Ψ_S is negative, so when $\Theta > 1$ also $\beta_S > \beta_0$.

Because the pre-sheath is quasi-neutral the dynamic ion density decrease must not exceed the electron density decrease. Since the Bohm criterion is not fulfilled in the pre-sheath [24], there must exist in the pre-sheath a mechanism that compensates the ion density decrease caused by the acceleration of the ions in the pre-sheath. It is beyond the scope of this paper to analyze such mechanisms in detail. Instead we again only quote the result of Riemann [24]. This result is the following. When the ions are cold ($T_i = 0$), like in our case, in the pre-sheath either (i) the ion current density increases, and/or (ii) the total ion energy decreases due to a retarding force. The increase of the ion current density can be caused either by: (1) the concentrating geometry, like spherical or cylindrical, where the ion trajectories converge towards the sheath edge and/or (2) volume ionization in the pre-sheath. On the other hand the retarding force that causes the loss of energy of the ions in the pre-sheath is due to elastic collisions of the ions with other types of particles like electrons and neutrals. In a fully ionized plasma the ions can exchange momentum only with electrons. In a weakly ionized plasma the ions loose their energy also by the collisions with neutrals.

In our one-dimensional model we treat an infinitely large planar electrode in an unmagnetized plasma. So we have a planar geometry and the geometric effects can not cause the ion current density increase. The remaining mechanisms are therefore the decrease of the total ion

$$M = \sqrt{\frac{1+\beta_S(M)+G(M)}{\left(1-\frac{J_R+M\gamma_i}{\sqrt{N^2-\frac{2\Psi_C}{\mu}}}\right)\left(1+\frac{\beta_S(M)}{\Theta}\right)+\frac{G(M)+\frac{(1+\beta_S(M))(J_R+M\gamma_i)}{\sqrt{N^2-\frac{2\Psi_C}{\mu}}}}{2\left(\Psi_C-\frac{N^2\mu}{2}\right)}}} \equiv f(M), \tag{39}$$

energy due to a retarding force caused by the momentum exchange collisions of the ions with electrons and neutrals and the volume ionization and recombination in the pre-sheath. The ion continuity equation for a stationary pre-sheath in one dimension can be written in the following way:

$$v_i \frac{dn_i}{dx} + n_i \frac{dv_i}{dx} = S_i. \tag{31}$$

Here S_i the ion source term, which gives the difference between the number of created and destroyed ions per unit volume and per time unit due to collisions between the electrons and the neutrals and the electrons and the ions. The equation of motion for ions in one dimension reads:

$$m_i v_i \frac{dv_i}{dx} + e_0 \frac{d\Phi}{dx} = -R_i - \frac{m_i v_i}{n_i} S_i, \tag{32}$$

where R_i is the effective ion friction force caused by the momentum transfer collisions between the ions and the electrons and between the ions and the neutrals. This force is usually written in the following form:

$$R_i = m_i \sum_k \nu_{ik} \left(v_i - v_k\right),$$

where ν_{ik} is the frequency for momentum exchange collisions between the ions and the species of type k. In our case the summation over k would include electrons and neutrals.

Equations (27), (32) and (31) form a system of 3 equations for $\Phi(x)$, $v_i(x)$ and $n_i(x)$. The boundary conditions are given by the values of Φ, n_i and v_i, at the sheath edge, which are Φ_S, v_0 (Eq. (6)) and n_S. It is of course beyond the scope of this paper to analyze the system of equations (27), (32) and (31). Instead we only note the following. The ion fluid equation of motion (32) can be multiplied by dx and integrated:

$$\frac{m_i v_i^2(x)}{2} + e_0 \Phi(x) = -\int \left(R_i + \frac{m_i v_i}{n_i} S_i\right) dx. \tag{33}$$

The integral on the right hand side of equation (33) can only be done if the system (27), (32) and (31) is solved and $v_i(x)$ and $n_i(x)$ are found. So we are now forced to make an oversimplification in order to find a relation between v_0 and Φ_S. We assume that at a very large distance from the collector ($x \geq L$) the ion velocity is zero and the potential there is also zero. At the sheath edge the ion velocity is v_0 and the potential is Φ_S. These two values are inserted into (33) and the integral on the right hand side is replaced by E_c which is an average energy loss of an ion caused by the collisions in the pre-sheath. E_c is treated as a constant parameter. Equation (33) turns into:

$$e_0 \Phi_S + \frac{1}{2} m_i v_0^2 + E_c = 0. \tag{34}$$

From (34), (6) and (8) it is straightforward to calculate the potential drop in the pre-sheath:

$$\Psi_S = -\frac{M^2}{2} - \varphi, \tag{35}$$

where

$$\varphi = \frac{E_c}{kT_1}. \tag{36}$$

From (30) we then obtain:

$$\beta_S(M) = \beta_0 \exp\left(\frac{\left(M^2+2\varphi\right)(\Theta-1)}{2\Theta}\right). \tag{37}$$

So β_S becomes a function of M. When (37) is inserted into the auxiliary emission coefficient G defined in (17), G also becomes a function of M:

$$G(M) = \frac{\gamma\left(\exp(\Psi_C) + \beta_0 \exp\left(\frac{\left(M^2+2\varphi\right)(\Theta-1)}{2\Theta}\right)\sqrt{\Theta}\exp\left(\frac{\Psi_C}{\Theta}\right)\right)}{\sqrt{2\pi(N^2\mu - 2\Psi_C)}}. \tag{38}$$

When (37) and (38) are inserted into the Bohm criterion (26) the later becomes a transcendental equation for M, which can be solved numerically if the other parameters are known:

see equation (39) above

where $\beta_S(M)$ is given by (37) and $G(M)$ is given by (38). Solving equation (39) for M means finding the intersection between the straight line $M = M$ and the function $f(M)$ defined on the right hand side of equation (39).

2.4 Critical electron emission

It is known that:

$$\frac{1}{2}\frac{d}{dz}\left(\frac{d\Psi}{dz}\right)^2 = \frac{d\Psi}{dz}\frac{d^2\Psi}{dz^2}.$$

The Poisson equation (18) is multiplied by $d\Psi/dz$. In this way differentials dz cancel out and equation (18) is

integrated once over Ψ from 0 to Ψ_C:

$$\frac{1}{2}\left(\frac{d\Psi}{dz}\right)^2_{\Psi=\Psi_C} = \frac{1}{1+\beta_S+G} \times \left[\begin{array}{l} \left(\exp(\Psi_C) - 1 + \beta_S\Theta\left(\exp\left(\frac{\Psi_C}{\Theta}\right)-1\right)\right) \\ \times\left(1-\frac{J_R+M\gamma_i}{\sqrt{N^2-\frac{2\Psi_C}{\mu}}}\right) + 2\left(G+\frac{(1+\beta_S)(J_R+M\gamma_i)}{\sqrt{N^2-\frac{2\Psi_C}{\mu}}}\right) \\ \times\left(\Psi_C-\frac{N^2\mu}{2}\right)\left(1-\sqrt{1-\frac{\Psi_C}{\Psi_C-\frac{N^2\mu}{2}}}\right) \end{array}\right] - M^2\left(1-\sqrt{1-\frac{2\Psi_C}{M^2}}\right). \quad (40)$$

Equation (40) enables one to calculate the electric field at the collector if all the other parameters are known. On the left hand side of equation (40) the boundary condition (2) has been taken into account. Note that β_S is given by (37), G is given by (38) and M is given by (39).

If the emission of electrons from the collector increases, eventually the density of the emitted electrons and consequently the negative space charge in front of the collector becomes so high, that the electric field at the collector becomes zero. When this happens, the left hand side of equation (40) is equal to zero. Equation (40) with the left hand side equal to zero is called the zero electric field condition at the collector.

2.5 Current to the collector

Next we would like to find an expression for the electric current density to the collector as a function of the collector potential. Using the same normalizing current density as in equation (17) the fluxes (13)–(15) can be written in the following dimensionless form:

$$J_e^{(1)} = \frac{1}{\sqrt{2\pi\mu}}\frac{1-\frac{J_R+M\gamma_i}{\sqrt{N^2-\frac{2\Psi_C}{\mu}}}}{1+\beta_S+G}\exp\left(\Psi_C\right), \quad (41)$$

$$J_e^{(2)} = \frac{\beta_S\sqrt{\Theta}}{\sqrt{2\pi\mu}}\frac{1-\frac{J_R+M\gamma_i}{\sqrt{N^2-\frac{2\Psi_C}{\mu}}}}{1+\beta_S+G}\exp\left(\frac{\Psi_C}{\Theta}\right), \quad (42)$$

$$J_e^{(3)} = \frac{G\sqrt{N^2-\frac{2\Psi_C}{\mu}}+(1+\beta_S)(J_R+M\gamma_i)}{1+\beta_S+G}, \quad (43)$$

$$J_i = M. \quad (44)$$

The total current density J_t is a sum of all 4 contributions. Equations (41)–(44) give absolute values of the current densities of individual particle species. In order to find the total current density J_t the fluxes J_i, $J_e^{(1)}$, $J_e^{(2)}$ and $J_e^{(3)}$ must be taken with the appropriate sign. In order to obtain the current in the technical direction, consistent with Figure 1 we take $J_e^{(1)}$ and $J_e^{(2)}$ with the positive sign and J_i and $J_e^{(3)}$ with the negative sign:

$$J_t = J_e^{(1)} + J_e^{(2)} - J_e^{(3)} - J_i = \frac{1}{1+\beta_S+G} \times \left[\begin{array}{l} \frac{1-\frac{J_R+M\gamma_i}{\sqrt{N^2-\frac{2\Psi_C}{\mu}}}}{\sqrt{2\pi\mu}}\left(\exp\left(\Psi_C\right)+\beta_S\sqrt{\Theta}\exp\left(\frac{\Psi_C}{\Theta}\right)\right) \\ -\left(G\sqrt{N^2-\frac{2\Psi_C}{\mu}}+(1+\beta_S)(J_R+M\gamma_i)\right) \end{array}\right] - M. \quad (45)$$

Again β_S is given by (37), G is given by (38) and M is given by (39) so that expressions (41)–(45) are much longer and more complicated as they seem at a first glance.

3 Results

In an experiment the hot to cool electron density and temperature ratio at a large distance from boundary electrodes is determined by the plasma production. Usually the density of the energetic electron population is smaller than the density of the cool electrons. Because of that we shall only consider the case when $\beta_0 < 1$ in this work. On the other hand the temperature of the hot electrons can be rather high. In this work we will present the results of the model with the selected values of Θ up to 50, but also higher values, up to several hundred could in principle be considered. The mass of ions is determined by the choice of gas. In this work we show some results for hydrogen plasma ($\mu = 1/1836$), but also other gases could be analyzed.

The Richardson current density is determined by the temperature of the collector and the emission coefficient is given by the properties of the collector material. The velocity distribution function of the emitted electrons is usually not known, but very often they are treated as monoenergetic. We do the same in our model, but we allow the initial velocity v_C of the electrons at the collector to be different from zero. This velocity is selected as an independent parameter of the model. Monoenergetic emitted electrons are of course an idealization. In an experiment they always have some velocity distribution. If the electron emission is thermal and the temperature of the collector is T_C and v_C is set equal to the thermal velocity of electrons with the temperature T_C, we get:

$$v_C = \sqrt{\frac{kT_C}{m_e}} = N\sqrt{\frac{kT_1}{m_i}}, \quad N = \sqrt{\frac{T_C m_i}{T_1 m_e}}.$$

For $T_C = 2000$ K, $kT_1 = 1$ eV and hydrogen ions we get $N = 17.8$. In this way an orientation value for the order of magnitude of N that should be examined is obtained. The values of N between 0 and 90 are considered in this work in order to illustrate the effect of the nonzero initial velocity v_C of the emitted electrons.

The parameter φ gives an average value of the energy, normalized to the cool electron temperature, lost by the

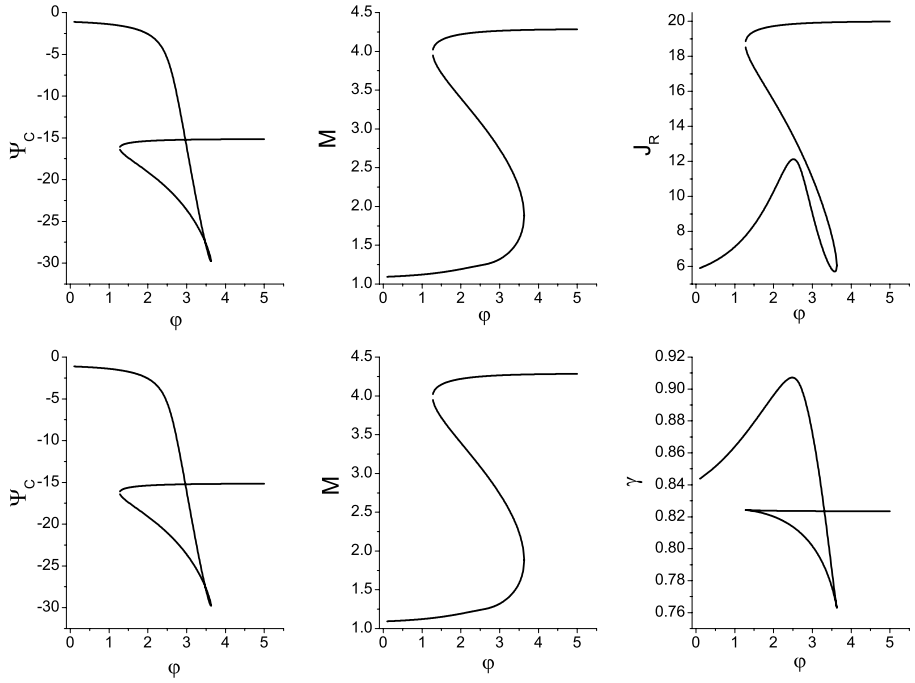

Fig. 2. In the top row Ψ_C, M and J_R found from the solutions of the system of equations (39), (40) and (45) are plotted versus φ. The other parameters are: $\beta_0 = 0.02$, $\Theta = 16$, $N = 0$, $\gamma_i = \gamma = 0$ and $\mu = 1/1836$. In the bottom row Ψ_C, M and γ found from the solutions of the system of equations (39), (40) and (45) are plotted versus φ. In this case the other parameters are: $\beta_0 = 0.02$, $\Theta = 16$, $N = 0$, $\gamma_i = J_R = 0$ and $\mu = 1/1836$.

ions because of the collisions that they suffer in the presheath. In an experiment such a parameter would be determined by the pressure and by the degree of ionization. In order to find out what are the relevant values of φ to be selected we do the following. We select $\beta_0 = 0.02$, $\Theta = 16$, $N = 0$, $\gamma_i = \gamma = 0$ and $\mu = 1/1836$ and we solve the system of equations (39), (40) and (45) for Ψ_C, M and J_R while we gradually increase φ. The total current density J_t in (45) and the derivative $d\Psi/dz$ in (40) are set to zero. So Ψ_C is the potential drop in the sheath that corresponds to the floating potential of the collector and J_R corresponds to the space charge limited (critical) electron emission. In this way plots of Ψ_C, M and J_R versus φ are obtained and they are shown in the top row of Figure 2. In the bottom row plots of Ψ_C, M and γ versus φ are shown. In this case Ψ_C, M and γ are found as the solutions of the same system of equations (39), (40) and (45) with the same parameters: $\beta_0 = 0.02$, $\Theta = 16$, $N = 0$ and $\mu = 1/1836$, only now $\gamma_i = J_R = 0$ is selected.

For small values of φ the system of equations only has 1 solution with M close to 1. As φ is increased Ψ_C decreases (becomes more negative) while M increases. J_R also increases but then reaches a maximum and starts to decrease. Similar is valid also for γ in the bottom right figure. When φ reaches a certain value φ_1, which in the case presented in Figure 2 is around 1.28 suddenly 2 additional solutions of the system of equations (39), (40) and (45) appear. One solution has M close to 4, which corresponds to $\sqrt{\Theta}$ and the other solution has M between 1 and $\sqrt{\Theta}$. It is convenient to distinguish the solutions by the corresponding Mach number M. In the view of the results shown in Figure 2 we will call the solution that is found for small values of φ and has M close to 1 the low solution. The solution with the largest M, which is close to $\sqrt{\Theta}$ will be called the high solution and the solution with the intermediate value of M will be called the medium solution. When φ exceeds a certain value φ_2, which in the case presented in Figure 2 is around 3.63, suddenly the low and the medium solution disappear and only the high solution remains. From the results shown in Figure 2 we conclude that relevant values of φ to be selected for the analysis of the results of the model may go up to 6 or 7. Note that when the system of equations (39), (40) and (45) is solved for the critical emission current density J_R with $\gamma_i = \gamma = 0$ or for the critical emission coefficient γ with $\gamma_i = J_R = 0$ the solutions for Ψ_C and M are in both cases identical.

We begin the presentation of the results of our model by the analysis of the Bohm criterion — equation (39). In Figure 3 we show the solutions of equation (39) for different values of the parameters β_0, Θ, φ, γ, N and J_R, while γ_i is always zero. These solutions are in fact the intersections between the curve $f(M)$ defined in (39) and the straight line $M = M$.

The parameters that are not changed in all 6 figures are $\mu = 1/1836$ (hydrogen plasma), $\Psi_C = -20$ and $\gamma_i = 0$. In the top left figure we select $\Theta = 25$, $\varphi = 0.1$, $J_R = 0$ and $\gamma_i = \gamma = 0$. Then $f(M)$ versus M curves are plotted for 3 different β_0. In the top middle figure we put $\beta_0 = 0.5$, $\varphi = 0.2$, $J_R = 0$ and $\gamma_i = \gamma = 0$ and we plot $f(M)$ versus M curves are plotted for 3 different Θ. In the top right figure the following parameters are selected: $\beta_0 = 0.02$, $\Theta = 20$, $\gamma_i = \gamma = 0$ and $J_R = 0$. Then $f(M)$ versus M curves are drawn for 3 different values of φ. In the bottom left figure we show $f(M)$ versus M curves for 3 values of J_R. The other parameters are: $\beta_0 = 0.1$, $\Theta = 20$, $\varphi = 0.1$, $\gamma_i = \gamma = 0$ and $N = 0$. In the bottom middle figure $f(M)$ versus M curves are shown for 3 values of γ. The other parameters are: $\beta_0 = 0.1$, $\Theta = 20$, $\varphi = 0.1$ and $\gamma_i = J_R = 0$. Finally in the bottom right figure we plot $f(M)$ versus M curves for 3 values of N, which are $N = 0$, $N = 45$ and $N = 90$.

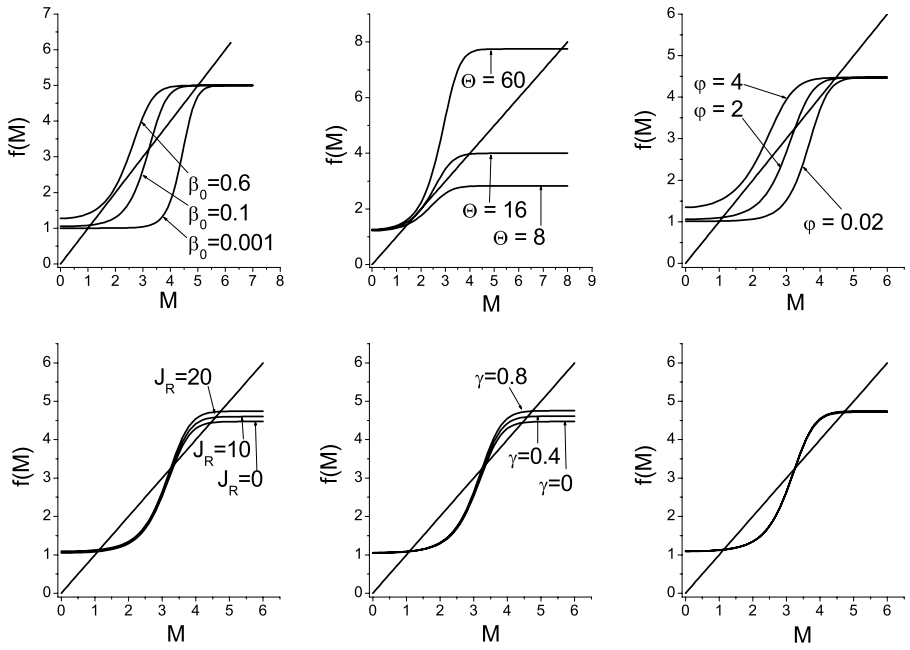

Fig. 3. Graphs of the function $f(M)$ defined in (39) for various values of parameters β_0, Θ, φ, γ, N and J_R. Parameters that are the same in all 6 figures are $\mu = 1/1836$ and $\Psi_C = -20$. The values of other parameters are given in the text.

The other parameters are: $\beta_0 = 0.1$, $\Theta = 20$, $\varphi = 0.1$, $J_R = 20$ and $\gamma_i = \gamma = 0$. The variation of N has almost no effect on $f(M)$ curves and the same is valid also for the variation of Ψ_C.

From the top 3 figures of Figure 3 one can see that the effect of β_0, Θ and φ to the solutions of equation (39) is similar. If the values of those 3 parameters are small, then equation the (39) only has 1 solution with M close to 1. This is the low solution. If they are large, then equation (39) again only has 1 solution, but this time with with M close to $\sqrt{\Theta}$. This is the high solution. For a wide range of values of β_0, Θ and φ equation (39) has 3 solutions with M close to 1, close to $\sqrt{\Theta}$ and with an intermediate value of M — the medium solution. On the other hand the emission parameters J_R, γ and N have much smaller impact on the $f(M)$ curves.

Now we proceed to analyze the current-voltage characteristics of the collector using the model presented in the previous section. In our model the plasma potential far away from the collector is set to zero. The collector potential Ψ_{col} is therefore a sum of the potential drop in the sheath Ψ_C and in the pre-sheath Ψ_S, $\Psi_{col} = \Psi_S + \Psi_C$. But for simplicity we take the potential drop in the sheath Ψ_C for the independent variable and in the figures we plot the current densities as functions of Ψ_C.

The current voltage characteristics $J_t(\Psi_C)$ is calculated in the following way. First the parameters β_0, Θ, μ, N and φ are selected. In this work we are interested in thermal electron emission from the collector, so we always put $\gamma_i = \gamma = 0$. The range of the selected values of β_0, Θ, μ, N and φ has been explained in the previous paragraphs. When the parameters are selected the boundary sheath potential drop Ψ_{CT}, where the transition between the space charge limited and the temperature limited emission for a given J_R occurs, must be found. This is done by solving the system of equations (39) and (40) for Ψ_{CT} and M. The derivative $d\Psi/dz$ on the left hand side of equation (40) is set equal to zero. Then Ψ_C is varied as an independent variable. For $\Psi_C \leq \Psi_{CT}$ (temperature limited emission) the Mach number M is found from (39) for every Ψ_C. Then the fluxes $J_e^{(1)}$, $J_e^{(2)}$, J_i and J_t are obtained using (41), (42), (44) and (45) respectively, while $J_e^{(3)}$ is equal to J_R for every $\Psi_C \leq \Psi_{CT}$. For $\Psi_C \geq \Psi_{CT}$ (space charge limited emission) the system of equations (39) and (40) is solved for M and J_R for every $\Psi_C \geq \Psi_{CT}$. Then the fluxes $J_e^{(1)}$, $J_e^{(2)}$, $J_e^{(3)}$, J_i and J_t are obtained from (41)–(45). For $\gamma_i = \gamma = 0$ the space charge limited current density $J_e^{(3)}$ given by the (43) is of course equal to J_R found from the system of equations (39) and (40).

In Figure 4 we show some properties of the solutions of the system of equations (39) and (40). The following parameters are selected: $\mu = 1/1836$, $\beta_0 = 0.124$, $\varphi = 0.2$, $N = 60$, $\gamma_i = \gamma = 0$ and $J_R = 21$, while Θ is gradually increased from 1 to 50. Every time the system of equations (39) and (40) is solved for Ψ_{CT} and M and the solutions are plotted versus Θ.

For small values of Θ the system of equations (39) and (40) only has the low solution. When Θ reaches a certain value, which is in this case around $\Theta \approx 13.2$, also the medium and the high solution of the system (39) and (40) appear. When Θ is further increased at approximately $\Theta \approx 27.5$, the low solution suddenly splits into 3 solutions so that the system of equations (39) and (40) has 5 solutions all together. Two additional solutions that appear after the low solution splits into 3 parts also belong to the low solution, because the corresponding M is close to 1. This splitting is shown in the bottom figures on an expanded scale.

In Figure 5 we show the dependence of the absolute value of the space charge limited emission current

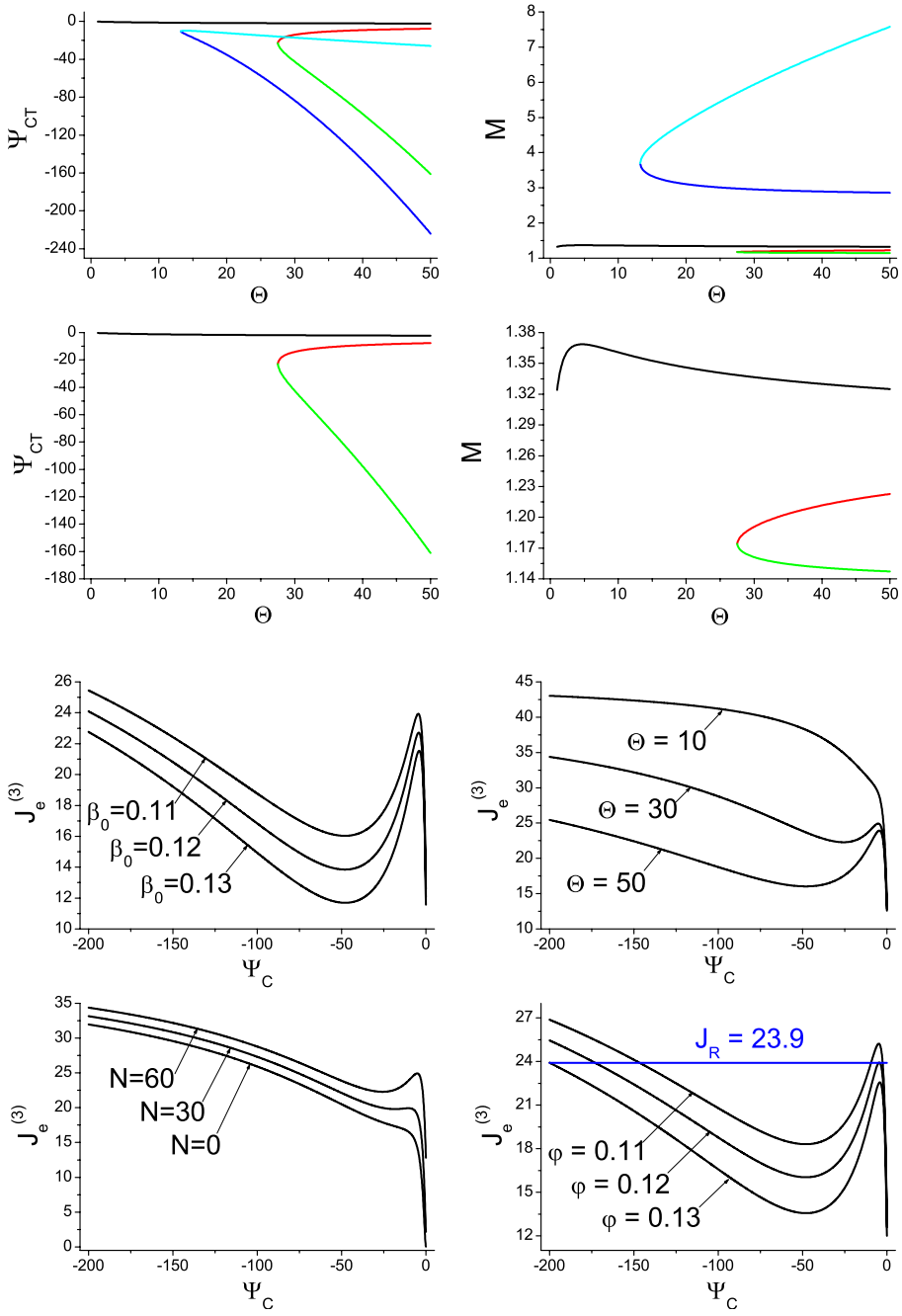

Fig. 4. (Color online) The solutions Ψ_{CT} and M of the system of equations (39) and (40) versus Θ. The other parameters are: $\mu = 1/1836$, $\beta_0 = 0.124$, $\varphi = 0.2$, $N = 60$, $\gamma_i = \gamma = 0$ and $J_R = 21$. In the bottom figures the splitting of the low solution is shown on an expanded scale.

Fig. 5. Absolute value of the space charge limited emission current density $J_e^{(3)}$ versus Ψ_C for different values of parameters β_0, Θ, N and φ. The values of the other parameters are given in the text.

density $J_e^{(3)}$ on Ψ_C. For the top left figure we select $\mu = 1/1836$, $\Theta = 50$, $N = 60$, $\gamma_i = \gamma = 0$, $\varphi = 0.2$ and 3 different β_0 are selected. For each set of parameters equations (39) and (40) are solved for M and J_R. Because we have selected $\gamma_i = \gamma = 0$ the obtained J_R is equal to the space charge limited emission current density $J_e^{(3)}$. In the top right figure we put $\mu = 1/1836$, $\beta_0 = 0.11$, $N = 60$, $\gamma_i = \gamma = 0$, $\varphi = 0.2$ and 3 different Θ are selected. Similar is done in the bottom left figure, where we select: $\mu = 1/1836$, $\Theta = 30$, $\beta_0 = 0.11$, $\gamma_i = \gamma = 0$, $\varphi = 0.2$ and 3 different N are selected.

As we can see, the absolute value of the space charge limited current density $J_e^{(3)}$ as a function of Ψ_C can have a local maximum and a minimum, especially if the values of N and Θ are high. Solving the system of equations (39) and (40) means in fact finding the intersection of the $J_e^{(3)}(\Psi_C)$ curve with a selected value of J_R. In dependence on the choice of parameters one can have 1, 2 or even 3 solutions for Ψ_{CT}. This is illustrated in the bottom right of Figure 5, where $J_e^{(3)}(\Psi_C)$ is plotted for 3 different values of φ, while the other parameters are: $\mu = 1/1836$, $\beta_0 = 0.11$, $N = 60$, $\gamma_i = \gamma = 0$ and $\Theta = 50$. The line, which represents the Richardson current density $J_R = 23.9$ is also plotted in this figure. This line has 1 intersection with the $J_e^{(3)}(\Psi_C)$ curve when $\varphi = 0.13$, 2 intersections when $\varphi = 0.12$ and 3 intersections when $\varphi = 0.11$.

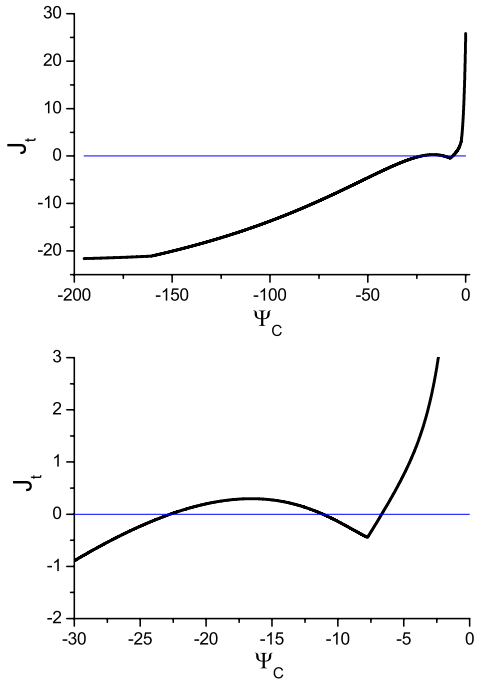

Fig. 6. The total current density J_t to the collector versus Ψ_C for the following parameters: $\mu = 1/1836$, $\beta_0 = 0.11$, $N = 60$, $\gamma_i = \gamma = 0$, $\varphi = 0.32$, $\Theta = 50$ and $J_R = 21$. Only the low solution of the system of equations (39) and (40) is considered. In the bottom figure the triple crossing of the zero current line (3 floating potentials) is shown on an expanded scale.

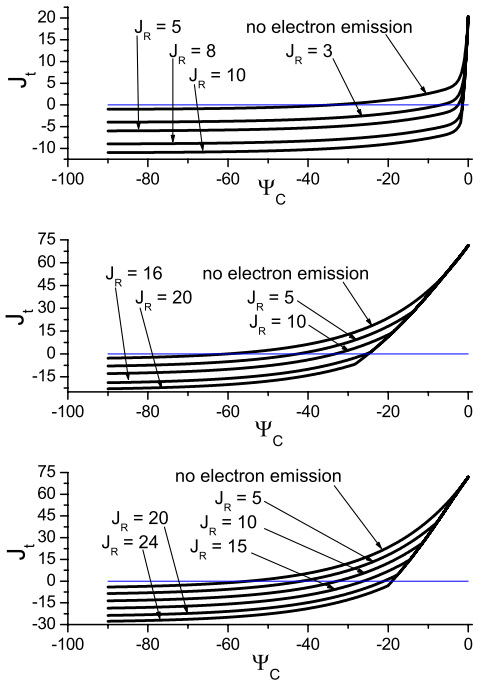

Fig. 7. Current density J_t to the collector versus Ψ_C for different values of J_R and the following parameters: $\mu = 1/1836$, $\beta_0 = 0.04$, $\gamma_i = \gamma = 0$, $N = 0$, $\varphi = 0.2$ and $\Theta = 20$. In the top figure the characteristics with M close to 1 are plotted, in the bottom figure the characteristics with M close to $\sqrt{\Theta}$ are plotted, and in the middle figure the characteristics that belong to the medium solution of the system of equations (39) and (40) are plotted.

Table 1. Solutions of the system of equations (39) and (40) for $\mu = 1/1836$, $\beta_0 = 0.11$, $N = 60$, $\varphi = 0.32$, $\Theta = 50$, $\gamma_i = \gamma = 0$ and $J_R = 21$.

Ψ_{CT}	M
–2.24012	1.3253
–7.75204	1.22179
–160.621	1.14692
–25.8833	7.57701
–223.926	2.86203

From the bottom right of Figure 5 we see the following. If J_R is smaller than the local minimum of $J_e^{(3)}(\Psi_C)$, then Ψ_{CT} is very close to zero and almost the entire current voltage characteristics is in the temperature limited regime. If J_R is larger than the local maximum of $J_e^{(3)}(\Psi_C)$, then Ψ_{CT} is very negative and almost the entire current voltage characteristics is in the space charge limited regime. If J_R is between the local minimum and the local maximum of the $J_e^{(3)}(\Psi_C)$ curve, then one must take care of the transitions between space charge limited and temperature limited emission, when calculating the characteristics.

This is illustrated in Figure 6, where the total current density J_t is plotted versus Ψ_C. The following parameters are selected: $\mu = 1/1836$, $\beta_0 = 0.11$, $\varphi = 0.32$, $N = 60$, $\Theta = 50$,$\gamma_i = \gamma = 0$ and $J_R = 21$. For these parameters the system of equations (39) and (40) has 5 solutions for Ψ_{CT} and M that are given in Table 1.

When M is close to 1 the current voltage characteristics has 3 transitions between space charge limited and temperature limited emission that occur at potentials Ψ_{CT} given in Table 1. The $J_t(\Psi_C)$ curve crosses the zero line of J_t 3 times. This is shown in the bottom figure on an expanded scale. This means that for certain plasma parameters and electron emission fluxes the collector can have even 3 different floating potentials. In Figure 6 these floating potentials are: $\Psi_{f1} = -22.7218$, $\Psi_{f2} = -11.1368$ and $\Psi_{f3} = -6.67303$. Ψ_{f1} and Ψ_{f2} are in the space charge limited region and Ψ_{f3} is in the temperature limited region. The floating potential are found by solving the system of equations (39) and (45), where J_t in equation (45) is equal to zero.

The Richardson emission current density J_R has strong impact to the floating potential. We show this in Figure 7 where the current voltage characteristics for several J_R are plotted. The other parameters are kept constant: $\mu = 1/1836$, $\beta_0 = 0.04$, $\varphi = 0.2$, $\gamma_i = \gamma = 0$, $N = 0$ and $\Theta = 20$. They are selected so that the space charge limited emission current $J_e^{(3)}$ is a monotonous function of Ψ_C and the system of equations (39) and (40) only has 3 (and not 5) solutions. As J_R increases also the floating potential increases (becomes less negative), while the boundary potential Ψ_{CT} between the temperature limited and space charge limited emission decreases (becomes more negative). At certain J_R they become equal. If J_R is

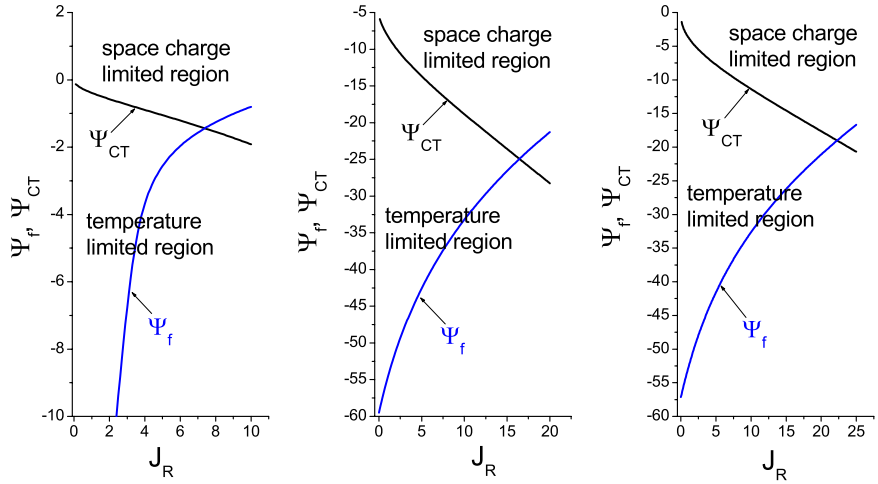

Fig. 8. The floating potential Ψ_f and the boundary potential Ψ_{CT} between the space charged limited and the temperature limited emission versus J_R for the following parameters: $\mu = 1/1836$, $\beta_0 = 0.04$, $N = 0$, $\gamma_i = \gamma = 0$, $\varphi = 0.2$, and $\Theta = 20$. In the left figure the low solution in the middle figure the medium solution and in the right figure the high solution of the system of equations (39) and (40) is shown. Below the $\Psi_{CT}(J_R)$ curve is the region of temperature limited emission and above this curve is the region of space charge limited emission.

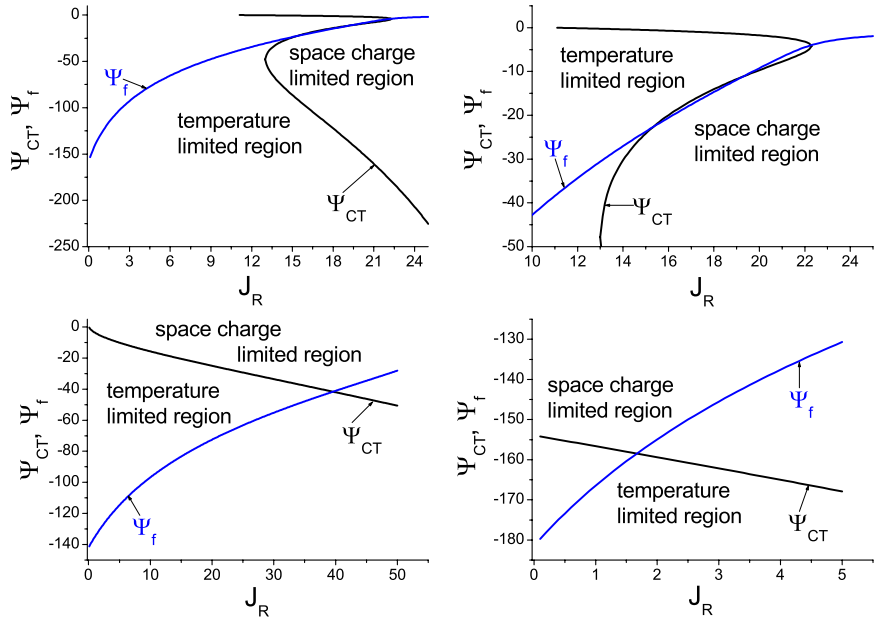

Fig. 9. The floating potential Ψ_f and the boundary potential Ψ_{CT} between the space charged limited and temperature limited emission versus J_R for the following parameters: $\mu = 1/1836$, $\beta_0 = 0.11$, $N = 60$, $\gamma_i = \gamma = 0$, $\varphi = 0.32$ and $\Theta = 50$. In the top left figure the low solution of the system of equations (39) and (40) is shown. In the top right figure the intersections between the Ψ_f and the Ψ_{CT} curve are shown on an expanded scale. In the bottom left figure the high solution is illustrated and in the bottom right figure the medium solution is plotted.

further increased, the floating potential can not increase any more, because it must not exceed the boundary potential of the space charge limited emission. So even if J_R further increased, the floating potential Ψ_f remains constant.

We illustrate this in Figure 8 where we plot the boundary potential Ψ_{CT} between the space charge limited and the temperature limited emission and the floating potential Ψ_f versus J_R for the same parameters that have been selected also in Figure 7 and they are the following: $\mu = 1/1836$, $\beta_0 = 0.04$, $\gamma_i = \gamma = 0$, $N = 0$, $\varphi = 0.2$ and $\Theta = 20$. The curves of the boundary potential $\Psi_{CT}(J_R)$ are found by solving the system of equations (39) and (40) for M and Ψ_C, while J_R is gradually increased. The curve of the floating potential $\Psi_f(J_R)$ is found by solving the system of equations (39) and (45) for M and Ψ_C, while J_R is gradually increased. We put $J_t = 0$ in equation (45).

For the selected parameters both systems of equations, namely the system of equations (39) and (40), as well as the system of equations (39) and (45) only have 3 solutions. For the low solution Ψ_f and Ψ_{CT} become equal at $\Psi_f = \Psi_{CT} = -1.43944$ and $J_R = 7.39151$. This is plotted in the left of Figure 8. In the middle of Figure 8 the medium solution is plotted. In this case Ψ_f and Ψ_{CT} become equal at $\Psi_f = \Psi_{CT} = -24.9379$ when $J_R = 16.4546$. In the right of Figure 8 the high solution is shown. In this case Ψ_f and Ψ_{CT} become equal at $\Psi_f = \Psi_{CT} = -19.0192$ with $J_R = 22.2661$. The intersections of the $\Psi_{CT}(J_R)$ and $\Psi_f(J_R)$ curves are found by solving the system of equations (39), (40) and (45) for M, Ψ_C and J_R. The $\Psi_{CT}(J_R)$ curve divides the $\Psi_{CT} - J_R$ plane in two regions. Below the $\Psi_{CT}(J_R)$ curve is the region of temperature limited electron emission and above this curve there is the region of space charge limited electron emission.

In Figure 9 we show again the dependence of Ψ_{CT} and Ψ_f on J_R, only now we select the same parameters as in Figure 6, which are: $\mu = 1/1836$, $\beta_0 = 0.11$, $\gamma_i = \gamma = 0$, $N = 60$, $\varphi = 0.32$ and $\Theta = 50$. For these parameters

the system of equations (39) and (40) has 5 solutions, while the system of equations (39) and (45) only has 3 solutions. In the top left figure we show the low solution. As J_R increases the $\Psi_f(J_R)$ curve starts in the temperature limited region then goes into the space charge limited region, then returns into the temperature limited region and then it goes into the space charge limited region. The intersections of the $\Psi_{CT}(J_R)$ and $\Psi_f(J_R)$ curves occur at potentials Ψ_f and Ψ_{CT} equal to –22.7218, –11.1368 and –4.02174. The respective emission currents J_R are equal to 15.309, 19.29 and 22.2677. These intersections are shown in the top right figure on an expanded scale. In the bottom left figure the high solution is shown. The $\Psi_{CT}(J_R)$ and $\Psi_f(J_R)$ curves intersect at $\Psi_f = \Psi_{CT} =$ –41.6571 and $J_R = 39.5771$. In the bottom right figure the medium solution is shown. The $\Psi_{CT}(J_R)$ and $\Psi_f(J_R)$ curves intersect at $\Psi_f = \Psi_{CT} =$ –158.466 and $J_R = 1.66944$.

4 Conclusions

We have analyzed the formation of the plasma potential in front of a negative electrode that emits electrons and is immersed in a two electron temperature plasma by a simple one dimensional fluid model. The model is based on the approximation that the sheath thickness is much larger than the Debye length but in the same time also much smaller than the characteristic length of the pre-sheath. Inside the sheath the Boltzmann distribution of the hot and of the cool electrons is assumed. The ions and the emitted electrons are assumed to be monoenergetic. Energy and flux conservation of all 4 particle species in the sheath is also assumed. In order to estimate the potential drop in the pre-sheath several simplifications are made. The hot and the cool electrons are assumed to be Boltzmann distributed also in the pre-sheath. Also the density of the emitted electron in the pre-sheath is is assumed to be a known function of the potential. This function does not need to be specified, because we don't actually solve the Poisson equation in the pre-sheath. In the planar geometry of our model the two mechanisms that compensate the dynamic ion density decrease caused by the acceleration of the ions in the pre-sheath are the momentum exchange collisions of the ions with the neutrals and the electrons and the creation and the destruction of ions by ionization and recombination. The energy that the ions lose through both these mechanisms is treated in our model as a single independent parameter.

The presence of the hot electrons in the plasma has several effects. The first one is that there are two different potential drops possible in the pre-sheath region at the same plasma parameters far away from the electrode. The model predicts 3 different possible velocities of the ions at the sheath edge. One of them is determined by the hot electron temperature the second is determined by the cool electron temperature and the third one is intermediate. Multiple solutions for the velocity of ions at the sheath entrance when 2 groups of negative particles are present in the plasma have been found also by some other authors [12–14]. This result is in agreement with a well known fact that a spontaneous formation of current-free double layers [28] in a plasma is possible, when there is more than 1 group of negative particles present in the plasma. Such double layers have been observed in computer simulations [7,13,29] and experiments [30–32].

Another consequence of the presence of the hot electrons in the plasma is that the space charge limited electron emission current may have a very pronounced local minimum and maximum when regarded as a function of the electrode potential. This only happens when the pre-sheath potential drop is determined by the cool electrons and it usually happens when the hot electron temperature is a bit elevated (roughly at least approximately 30 times higher than the cool electron temperature). A nonzero initial velocity of emitted electrons also has an impact on the maxima and minima of the critical electron emission current. If the initial velocity of the emitted electrons is increased, the local maximum and minimum of the critical electron emission current appear at lower temperature of the hot electrons. For some values of β_0, Θ, N and J_R the current voltage characteristics of the electrode can cross the zero collector current line up to 3 times. This means that the floating potential of the electrode may have up to 3 different values. Triple valued floating potential can be found in rather narrow intervals of hot to cool electron density and temperature ratios. Three floating potentials of an electron emitting electrode immersed in a plasma with energetic electrons have been observed experimentally by Nam et al. [26] and also by Griskey and Stenzel [27]. In both these papers the electron emission from the electrode was secondary — caused by the impact of energetic electrons from the plasma. We have on the other hand in this work focused our attention to the current-voltage characteristics of an electrode with thermal emission of electrons. Nevertheless one of our main results — namely the triple floating potential of an electron emitting electrode — is rather similar to those reported in [26,27]. Our model can also be used for the analysis of the current-voltage characteristics of an electrode with secondary emission of electrons, when this emission is triggered either by the impacting electrons and/or ions and also for the situation when both (thermal and secondary) electron emission mechanisms are present.

In this work we have studied the transition between the space charge limited and the temperature limited electron emission. The obtained results could be relevant for the emissive probe applications in spite of the fact that the geometry of our model is planar, while the emissive probes are usually thin wires and therefore the cylindrical geometry would be more appropriate. Models with planar geometry [17] have been successfully applied for the analysis of the emissive probe characteristics. In an experiment one usually takes the floating potential of the emissive probe (which is measured with respect to some reference electrode) as the plasma potential. The actual plasma potential is somewhat more positive, but the difference is usually neglected. In our model we calculate the total flux to the collector J_t as a function of the potential drop in the sheath Ψ_C, which in our model is treated as

an independent variable. By analogy with the experiment, we should observe what happens with Ψ_C, where $J_t = 0$ (floating potential), when parameters β, Θ, N and J_R are varied. Variation of J_R in the model is analogous to the variation of the probe heating in the experiment. The simplest procedure for measurement of the plasma potential by an emissive probe is the following. The probe heating is gradually increased and the floating potential of the probe is measured. This potential increases with increased heating of the probe until a certain saturation value of the floating potential is reached. If the probe is further heated, the emission current still increases, but the floating potential does not change any more. Very often the probe heating is set somewhat above the saturation level, so that the emission current from the probe at strongly negative probe biases is approximately equal or somewhat larger (by the absolute value) than the current collected at the inflection point of the probe characteristics.

The results of our model are in agreement with this experimental practice. When J_R is increased (starting from zero), the sheath potential drop Ψ_f that corresponds to the floating collector increases (becomes less negative) and the sheath potential drop Ψ_{CT} where the transition between the space charge limited and the temperature limited emission occurs, decreases (becomes more negative). At certain J_R they become equal. If J_R was further increased, Ψ_f would become larger (less negative) than Ψ_{CT}. But for collector potentials that are larger (less negative) than Ψ_{CT}, the electron emission current is space charge limited and must be calculated from the zero electric field condition for every collector potential separately. Because of that the floating potential of the collector does not change any more even if J_R is further increased and a saturation of the floating potential is reached. The results of our model suggest that the saturation of the floating potential is achieved already at the values of J_R that are smaller than the values of J_t at $\Psi_C = 0$.

This work has been carried out within the Association EURATOM-MHST. The content of the publication is the sole responsibility of its authors and it does not necessarily represent the view of the Commission or its services. The authors would also like to thank to one of the referees who contributed considerably to the improvement of the paper.

References

1. N. Hershkowitz, IEEE Trans. Plasma Sci. **22**, 11 (1994)
2. G.D. Hobbs, J.A. Wesson, Plasma Phys. **9**, 85 (1967)
3. L.A. Schwager, Phys. Fluids B **5**, 631 (1993)
4. C.A. Ordonez, Phys. Rev. E **55**, 1858 (1997)
5. L. Jolivet, J.-F. Roussel, IEEE Trans. Plasma Sci. **30**, 318 (2002)
6. F. Taccogna, S. Longo, M. Capitelli, Phys. Plasmas **11**, 1220 (2004)
7. T. Gyergyek, M. Čerček, Czech. J. Phys. **54**, 431 (2004)
8. L. Schott, Phys. Fluids **30**, 1795 (1987)
9. S. Takamura, Phys. Lett. A **133**, 312 (1988)
10. N. Jelić, M. Čerček, M. Stanojević, T. Gyergyek, J. Phys. D: Appl. Phys. **27**, 2487 (1994)
11. S.B. Song, C.S. Chang, D. Choi, Phys. Rev. E, **55**, 1213 (1997)
12. K. Sato, F. Miyawaki, Phys. Fluids B **4**, 1247 (1992)
13. M. Čerček, T. Gyergyek, M. Stanojević, Contrib. Plasma Phys. **39**, 541 (1999)
14. F.A. Haas, N.St.J. Braithwaite, J. Phys. D: Appl. Phys. **33**, 72 (2000)
15. D. Tskhakaya, S. Kuhn, V. Petržilka, R. Khanal, Phys. Plasmas **9**, 2486 (2002)
16. M.Y. Ye, T. Shimada, T. Kuwabara, N. Ohno, S. Takamura, *Proceedings of the 1998 ICCP&25th EPS Conference on Controlled Fusion and Plasma Physics*, Praha, 29 June–3 July 1998, ECA **22C**, 23 (1998)
17. M.Y. Ye, S. Takamura, Phys. Plasmas **7**, 3457 (2000)
18. S. Takamura, N. Ohno, M.Y. Ye, T. Kuwabara, Contrib. Plasma Phys. **44**, 126 (2004)
19. Y. Hagino, N. Ohno, S. Takamura, Contrib. Plasma Phys. **44**, 144 (2004)
20. T. Gyergyek, M. Čerček, Contrib. Plasma Phys. **45**, 89 (2005)
21. T. Gyergyek, M. Čerček, Contrib. Plasma Phys. **45**, 568 (2005)
22. Yu.P. Raizer, *Gas Discharge Physics* (Springer Verlag, 1997)
23. K.U. Riemann, J. Seebacher, D.D. Tskhakaya Jr, S. Kuhn, Plasma Phys. Contr. Fusion **47**, 1949 (2005)
24. K.U. Riemann, J. Tech. Phys. **41**, 89 (2000)
25. K.U. Riemann, IEEE Trans. Plasma Sci. **23**, 709, (1995)
26. Cheol-Hee Nam, N. Hershkowitz, M.H. Cho, T. Intrator, D. Diebold, J. Appl. Phys. **63**, 5674 (1988)
27. M.C. Griskey, R.L. Stenzel, Phys. Rev. Lett. **82**, 556, (1999)
28. F.F. Chen, Phys. Plasmas **13**, 034502 (2006)
29. A. Meige, R.W. Boswell, C. Charles, M. Turner, Phys. Plasmas **12**, 052317 (2005)
30. G. Hairapetian, R.L. Stenzel, Phys. Fluids B **3**, 899 (1991)
31. C. Charles, R.W. Boswell, Phys. Plasmas **11**, 1706 (2004)
32. C. Charles, R.W. Boswell, Phys. Plasmas **11** 3808 (2004)